Medium-velocity superconducting cavity for high accelerating gradient continuous-wave hadron linear accelerators

K. McGee,[1] S. Kim,[1] K. Elliott,[1] A. Ganshyn,[1] W. Hartung,[1] E. Metzgar,[1] P. Ostroumov,[1]
L. Popielarski,[1] J. Popielarski,[1] A. Taylor,[1] T. Xu,[1] M. P. Kelly,[2] B. Guilfoyle,[2] and T. Reid[2]

[1]*Michigan State University, East Lansing, Michigan 48824, USA*
[2]*Argonne National Laboratory, Argonne, Illinois 60439, USA*

We present the first rf studies of the medium-β superconducting radio frequency (SRF) elliptical cavities designed for Michigan State University's Facility for Rare Isotope Beams (FRIB) energy upgrade linac. The proposed energy upgrade for this continuous-wave (CW) superconducting linac will double the final beam energy from 200 to 400 MeV/u for the heaviest uranium ions within the 80 m of space available in the FRIB tunnel. Two prototype $\beta_{opt} = 0.65$ 644 MHz five-cell elliptical SRF cavities were fabricated and tested to validate the novel cavity design with three conventional rf recipes: (1) Electropolishing (EP-only), (2) EP + 48 h 120 °C bake (EP + baking), and (3) Buffered chemical Polishing + 48 h 120 °C bake (BCP + baking). The EP-only recipe achieved a 2 K quality factor (Q_0) of 2.3×10^{10} at the FRIB energy upgrade design accelerating gradient (E_{acc}) of 17.5 MV/m, and Q_0 of 1.2×10^{10} at a maximum gradient of 26 MV/m, where the gradient was ultimately limited by the available rf amplifier power available for this test. These results validate the potential of the novel 644 MHz medium-β cavity design and motivate its use in future high-Q_0 development work. The multipacting band, which exists at $E_{acc} \approx 10$ MV/m, was completely conditioned in the continuous-wave mode. We also observed that combining the 48 h 120 °C baking treatment with EP did not improve the EP-only cavity performance at 2 K due to increased residual resistance (R_0) and increased medium-field Q-slope. BCP + baking was also found to produce lower Q_0 in this cavity due to increased medium-field Q-slope. The mechanical modes of this cavity were measured at room temperature, verifying that the quality factor of the dominant "accordion" mechanical mode these medium-β cavities are particularly vulnerable to is close to that of the 1.3 GHz TESLA cavities. Thus, this mode arising from the novel geometry of these cavities is shown to not be of excessive concern for resonance control.

I. INTRODUCTION

To meet the FRIB energy upgrade project (FRIB400 [1]) design specifications, multiple cavity designs and operating frequencies were investigated. With all cavity options scaled to a peak electric field of 40 MV/m, it was determined that a novel five-cell elliptical 644 MHz cavity with $\beta_{opt} = 0.65$ was the only one able to achieve 400 MeV/u for uranium ions within the 80 m available in the FRIB linac tunnel [2]. This design minimized numbers of additional cavities and cryomodules needed, provided the cavities can be processed to achieve E_{acc} of 17.5 MV/m with a Q_0 of at least 2×10^{10}. This cavity design also achieves the lowest total dynamic heat load in

the upgraded linac segment [2]. A summary of fundamental parameters for this cavity is presented in Table I.

With the design established, the goal of this work is to validate that the novel FRIB400 cavity has good potential to serve as a testbed for high-Q recipe development. We thus seek to demonstrate that reasonable rf performance can be achieved with at least one of the number of conventional rf surface processing recipes. Technologies for processing superconducting radio frequency (SRF) cavities have matured over a wide range of operating frequencies and velocities. With multiple applications and the inertia provided by a long history in the literature, the 1.3 GHz TESLA cavities have persisted as the testbed of choice for novel high-gradient and high-Q cavity processing treatments [3]. In these cavities, electropolishing (EP) [4] evolved into the "standard ILC" treatment developed for the International Linear Collider (ILC) [5]. In the context of mass-production for the European X-ray Free Electron Laser, the ILC recipe was shown to be highly repeatable on over 800 1.3 GHz SRF cavities, with the average cavity

TABLE I.   Cavity specifications.

Parameter	Value	Units
Frequency	644	MHz
Geometrical β	0.61	
Optimal β	0.65	
Aperture diameter	83	mm
Effective length L_{eff}	71.0	cm
Number of cells	5	
Geometric shunt impedance R/Q	368	Ω
Geometry factor G	188	Ω
E_{peak}	40	MV/m
B_{peak}	77.5	mT
Accelerated gradient E_{acc}	17.5	MV/m
$E_{\text{peak}}/E_{\text{acc}}$	2.28	
$B_{\text{peak}}/E_{\text{acc}}$	4.42	mT/(MV/m)

gradient exceeding specifications by 25% [6]. Initial explorations of nitrogen-doping (N-doping) [7] and nitrogen-infusion [8] for high-Q applications are also rooted in TESLA cells, and have seen early success and rapid industrialization for the Linac Coherent Light Source-II (LCLS-II) high-β 1.3 GHz cavities with improved Q at 2 K [9,10]. Low-velocity ($\beta_{\text{opt}} = \text{v}/\text{c} < 0.5$) cavity designs and surface treatments have also been well optimized. The EP-treated performance of low-β coaxial cavities is approaching state-of-the-art performance of the TESLA cavities processed with the standard ILC recipe [11]. In addition to EP, buffered chemical polishing (BCP) has also seen success in low-β cavities: in the recent baseline production cycle of approximately 300 $\beta_{\text{opt}} = 0.04$ to 0.53 quarter-wave and half-wave resonators for FRIB, BCP consistently met or exceeded all facility specifications [12,13].

Previous Q_0 development in this medium-β operating regime aimed at Q_0 requirements around an order of magnitude lower than the FRIB400 minimum requirements. The Spallation Neutron Source (SNS) specifications call for $Q_0 \geq 5 \times 10^9$ at $E_{\text{acc}} = 10.1$ MV/m for $\beta = 0.61$ cavities, and the European Spallation Source (ESS) specifications call for $Q_0 > 5 \times 10^9$ at $E_{\text{acc}} = 16.7$ MV/m for $\beta = 0.67$ cavities. SNS and ESS both applied BCP treatments and achieved their respective minimum requirements. While achieving their specifications, the SNS and ESS cavities did not consistently achieve $Q_0 > 2 \times 10^{10}$ [14,15,16] required for the FRIB400 upgrade.

Furthermore, the size of the FRIB upgrade cavity presents technical challenges for BCP, given the need for effective cavity surface cooling, and adequate flow rate to avoid the formation of nitrogen dioxide bubbles on the cavity surfaces during BCP [17]. Moreover, BCP yields a surface roughness nearly an order of magnitude higher than EP, where differently oriented crystals experience preferential etching [17,18], which can make reaching higher gradients without field emission (FE) more challenging.

Validating the EP-only performance of this cavity is of principal interest for this work as this treatment serves as the baseline for N-doping. Acceptable EP performance will justify pursuit of N-doping development in this medium-β geometry. Technical challenges inherent to applying EP to medium-β cavities [19] will be discussed later. The standard ILC EP treatment, augmented with low-temperature baking to remove high-field Q-slope [20], has been extensively developed in 1.3 GHz high-β cavities to achieve high Q and high gradient. EP also showed good high-Q and high-gradient performance in lower-frequency high-β cavities such as SNS high-β ($\beta = 0.81$, 805 MHz) and Proton Improvement Plan II (PIP-II) high-β ($\beta = 0.92$, 650 MHz) cavities [21,22,23]. However, it is not obvious how the 644 MHz FRIB prototype cavities will respond to the ILC EP process.

Specifically, cavity performance improves with the reduction of the rf surface resistance (R_s), which has temperature-dependent and temperature-independent parts (1) [24],

$$R_s = R_{\text{BCS}}(T) + R_0, \tag{1}$$

R_{BCS}, which is derived from the Bardeen-Cooper-Schrieffer theory of superconductivity, has key dependencies (2) on the operating frequency (ω), the superconducting energy gap (Δ), and the material parameter (A) [24],

$$R_s = \frac{A\omega^2}{T} e^{-\frac{\Delta}{k_B T}} + R_0. \tag{2}$$

The residual resistance (R_0) depends on various factors such as flux trapping, surface defects, and impurity content. Different cavity surface treatments and different operating conditions such as frequency, temperature, and accelerating gradient, will affect the surface resistance. Moreover, the electrodynamic and physical properties of the larger, lower-frequency medium-β cavity make it difficult to predict how R_s will respond to different surface processing techniques.

Thus, with the two prototype cavities available to FRIB for testing, S65-001 and S65-002, we elected to begin with a trial of ILC-like EP with low-temperature baking in S65-001, and BCP with low-temperature baking in cavity S65-002. Anticipating eventual interest in N-doping these cavities, we then chose to reset S65-001 and test EP-only (no baking) to baseline future N-doped S65-001 performance.

II. SURFACE PROCESSING AND CAVITY PERFORMANCE

The initial surface treatment of S65-001 was based on the standard ILC recipe for EP with a modified hydrogen degassing step. The 150 μm bulk EP at Argonne National Laboratory (ANL) with the modified electrode resulted in an average of 199 μm of removal from the beam pipes

and an average of 149 μm from the equatorial regions. The cavity was then baked for the purpose of hydrogen degassing: first at 350 °C for 12 h, then at 600 °C for 10 h. The cavity was then mechanically tuned to 97% cell-to-cell field flatness and shipped back to ANL for the final 20 μm EP, high-pressure water rinsing and clean assembly. For the ensuing EP + baking test and after the final clean assembly, S65-001 was baked at 120 °C for 48 h *in situ*, i.e., while assembled to the dunk-test insert and under vacuum. For the EP-only test, S65-001 was then "reset" using 40 μm EP at ANL, with the last 10 μm being "cold-EP" performed at 15–17 °C. High-pressure water rinsing (HPR) and clean assembly for this cavity was then conducted in FRIB cleanroom facilities.

Since test results of medium-β multicell cavities processed by EP have not been reported before, the process is worth describing, and in particular, the EP cathode geometry. The generic concern about the EP in the medium-β cavities is relatively high aspect ratio of the equator radius 197 mm to the iris-to-iris distance (single-cell length) 142 mm, compared to the other high-β cavities [2]. The greater distance of the cavity equator to the cathode, in general, effectively increases the electrolyte resistance, decreasing the cavity surface current as a function of position along the beam axis, which results in nonuniform surface removal [19]. To reduce this effect, the cathode at the position of the beam pipes and irises was masked with Teflon tape as shown in Fig. 1(a). Additional attachments, so-called doughnuts as shown in Fig. 1(b), were assembled onto the cathode at the position of the equators. The surface removal at the locations as shown in Fig. 1(a) was measured and the results are as shown in Fig. 1(c). The average surface removal at the equators is 75% of the average surface removal at the beam pipes. This ratio is reasonably high compared to not only medium-β single cell cavities but also TESLA cavities. However, the authors would like to note that it is possible that the surface removal around the irises, which was not accessible for the ultrasonic thickness measurements due to the stiffening rings, was higher than the beam pipes due to closer proximity to the unmasked aluminum doughnuts.

S65-002 underwent BCP treatment in FRIB baseline production BCP facilities mounted vertically and without additional cooling beyond that provided by the acid itself [10]. The treatment cycle consisted of a 120 μm etch, 600 °C baking, another 20 μm BCP etch, and an *in situ* 120 °C bake for 48 h (BCP + baking).

The 2 K Q-curves for the two S65-001 tests, EP-only and EP + baking, are presented in Fig. 2(a). The EP-only treatment achieved Q_0 of 2.3×10^{10} at $E_{acc} = 17.5$ MV/m, exceeding the FRIB upgrade requirements. The maximum E_{acc} was 26.1 MV/m, limited by the available amplifier power in the test. The EP + baking treatment achieved Q_0 of 1.9×10^{10} at maximum gradient $E_{acc} = 17.5$ MV/m. This maximum gradient was limited in amplifier power by
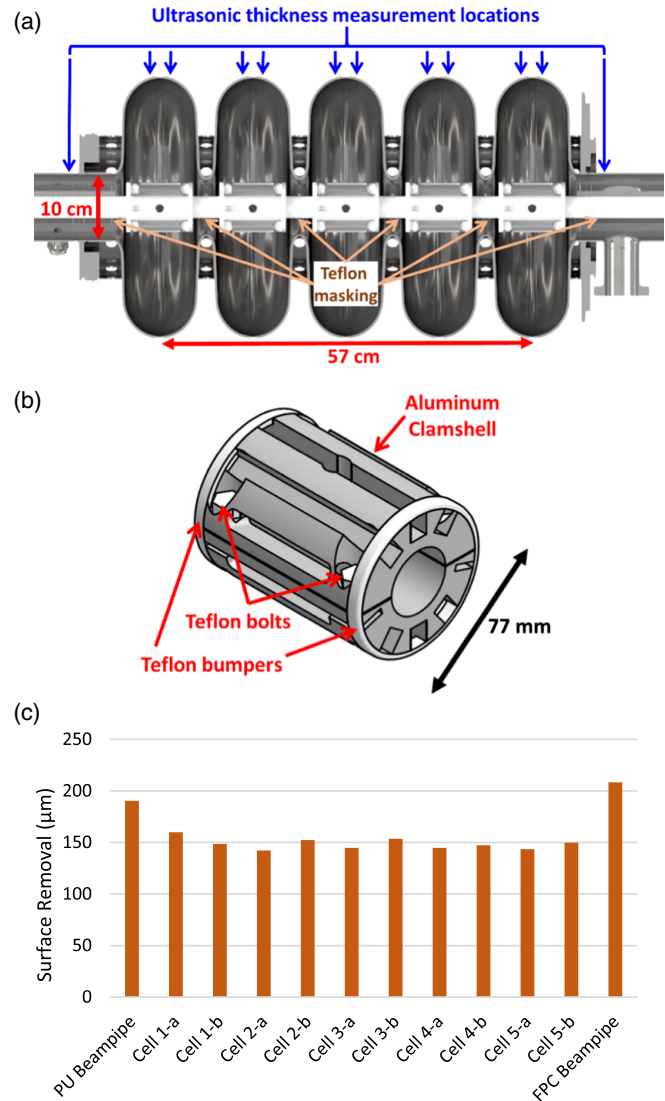

FIG. 1. S65-001 surface removal with bulk EP. (a) EP cathode integrated with the cavity. This also shows the doughnuts on the cathode at the equator locations and Teflon shielding at the iris locations. Red arrows indicate the locations for ultrasonic thickness measurements. (b) "Doughnut" to increase the cathode radius at the equator locations. Five doughnuts are attached to a cylindrical aluminum tube with 34 mm diameter; the remaining area of the aluminum tube is masked by Teflon tape. (c) Surface removal at the locations of the beampipes and equators. Since the outer surfaces of the irises were not easy to access due to stiffening rings, we measured the beampipes as a representation of the surfaces at a small radius. PU and FPC denote the pickup and fundamental power coupler, respectively.

unconditionable field emission. The measured field emission (FE) had negligible effect on Q_0, since it remained well below 100 mR/h at all fields. It has been found that FE must exceed 100 mR/h before causing measurable Q-drop [25]. Furthermore, the Q_0 observed at fields below 10 MV/m, a field level where FE was absent in all cavities tested, was the same between field-emitting and
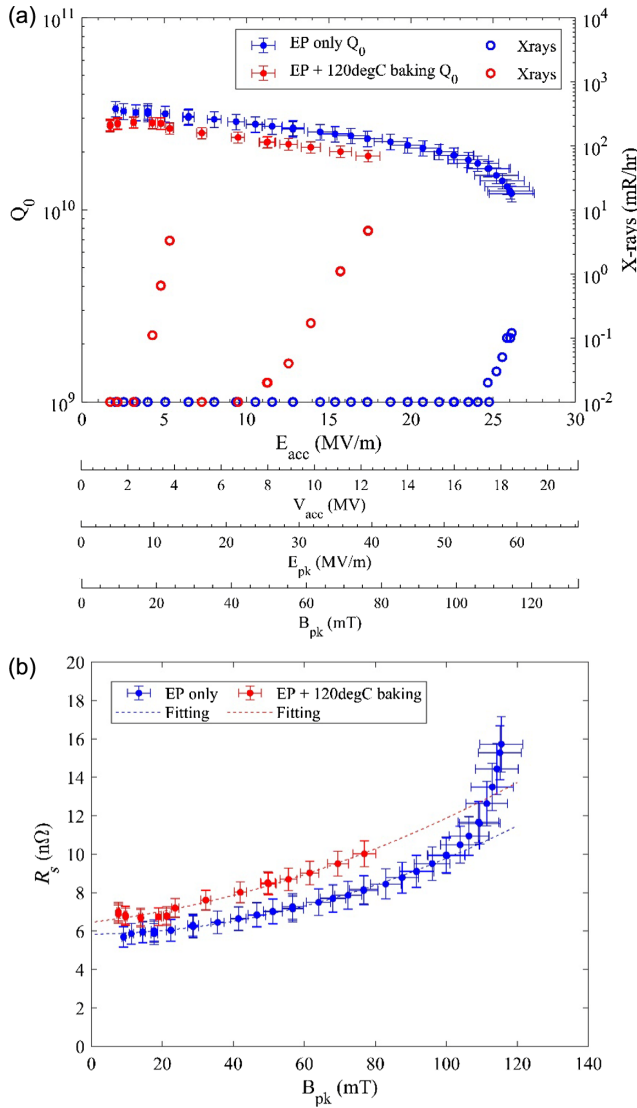
FIG. 2. Results of the high-power rf testing of 644 MHz $\beta_{opt} = 0.65$ cavities at MSU/FRIB. (a) 2 K Q curves comparing EP only vs EP + 120 °C baking recipes in S65-001. The blue circles are the EP-only case and the red circles are the EP + 120 °C baking case. The open circles are field-emission X rays, as read on the right-hand vertical scale. In all trials FE remained well below 100 mR/h, where noticeable degradation in Q due to FE ocurrs at 100 mR/h and above [25]. The color code is the same as for Q_0. (b) The same results as in (a) but scaled to show the rf surface resistance R_s. The dashed lines are second-degree polynomial fits to each data set. These fits were done for the data, for which B_{pk} is in the range of 20 to 100 mT, but they are extrapolated into the range of 1 to 120 mT for readability.

nonfield-emitting cavities. This suggests there was no inherent Q_0 degradation as a result of the presence of field-emitting contaminants. Given this, and the fact that the measured FE was below 100 mR/h, it was concluded that the presence of FE affected the maximum achievable gradient only, and had a negligible effect on measured Q_0. Further details regarding the relationship between Q_0 and

field emission are outside of the scope of this paper, and are thus not discussed.

The authors speculate that the contaminents resulting in this level of field emission originated in the HPR system, as presented in Sec. IV. Due to the limited spanning angle of the robotic arm, the HPR nozzle needed to have at least twelve holes to cover the entire cavity inner surface. This increase in hole humber from the two- to three-hole nozzles decreased the velocity of the water jets and thus lowered the impact force of the water against the cavity walls. The *in situ* baking of the cavity occurred after clean assembly, and thus is unlikely to have been the direct cause of the field emission.

In Fig. 2(b), these same results are presented in terms of the rf surface resistance (R_s) vs the peak magnetic field, B_{pk}, which more clearly shows the nature of the difference in R_s introduced by baking in EP-ed cavities. The baked cavity's R_s is increased above that of the unbaked cavity both by a slightly steeper slope in R_s vs B_{pk}, and an overall upwards shift, seen at low fields. As observed in Ref. [26], both linear and quadratic dependencies exist between R_s and field strength.

In general, the medium-field Q-slope is not solely affected by the intrinsic properties of the rf surface treatment. Extrinsic factors, such as localized defects or cavity contaminants also contribute. However, since this study encompasses the effect of baking on the FRIB400 cavity performance, we still find it useful to quantify the change in the Q-slope after the 120 °C *in situ* baking treatment. While all physical factors governing the medium- and high-field Q-slopes are not totally captured by a simple polynomial fit, it is instructive to compare our results to those presented in Ref. [26], which employed a second-order polynomial fit. This fitting further can shed light on what types of sources caused the additional losses after baking. Namely, if the losses originated from contaminations that caused excessive Joule heating or dielectric losses, we would be able to see an increase in the second-order term, regardless of how the contaminants are localized.

To aid to benchmarking the novel cavity's performance, we fit the data in Fig. 2(b) to the second-order polynomial equation:

$$R_s[\text{n}\Omega] = C_0 + C_1 b + C_2 b^2, \tag{3}$$

where b is normalized to B_{pk} defined by $b = B_{pk}/B_{pk,0}$, where $B_{pk,0}$ is the B_{pk} at the design accelerating gradient, 77.5 mT. C_0, C_1, and C_2 are respectively the zeroth-, first-, and second-order coefficients, which represent the relative strengths of field-independent, linear, and quadratic components of R_s at the design gradient. The fitting results are as shown in Table II. These results indicate that the zeroth- and first-order terms clearly contribute to the baked cavity's higher R_s at the operating gradient ($b = 1$).

TABLE II.   Second-order polynomial fitting results of the field-dependent R_s.

Case	C_0	C_1	C_2
EP-only	5.8 ± 0.023	0.15 ± 0.077	2.3 ± 0.052
EP + baking	6.5 ± 0.042	1.7 ± 0.19	1.9 ± 0.18

Figure 3 offers insight into the zeroth- and first-order terms. In plotting R_s vs T_c/T, the BCS resistance, R_{BCS}, is identified as the temperature-dependent decrease of R_s, and the residual resistance (R_0) is roughly identified with the temperature-independent (flat-line limit) of R_s at low T. The zeroth-order term contains the sum of the field-independent R_0 and the temperature-dependent R_{BCS}, however, at low temperatures (e.g., less than 2K) the overwhelming contribution to this term is R_0, and thus the zeroth-order term is largely taken to correspond to R_0, which is greater in the baked cavity (4). Near the right-hand edge of the plot in Fig. 3, we see that R_0 is not only greater in the baked cavity, but also the dominant contributor to R_s around 2 K, the FRIB operating temperature. Thus, even though baking visibly reduced R_{BCS}, this did not lead to better cavity performance at 2 K.

The first-order term, associated with the medium-field Q-slope (MFQS), can result from hysteresis losses due to Josephson fluxons formed at oxide-filled boundaries
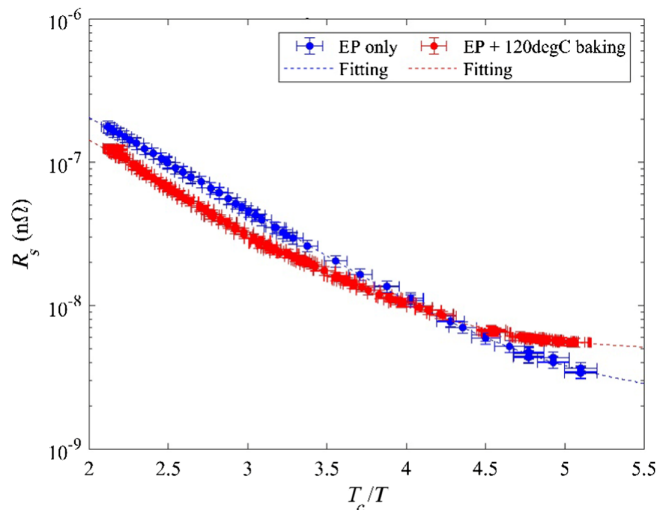

FIG. 3. R_s as a function of T_c/T, where $T_c = 9.2$ K, the critical temperature of niobium. T is taken as the liquid helium bath temperature. These data were recorded at constant E_{acc} of 2 MV/m for the EP-only case, and at approximately 4 MV/m for the EP + 120 °C baking case. This difference in field level is not regarded as significant because the total surface resistance, R_s, is relatively field independent at these low fields. Both datasets are fitted to Eq. (2), $R_s = \frac{A\omega^2}{T} e^{-\frac{\Delta}{k_B T}} + R_0$, where the fitted parameters are (1) EP-only: $A = 2.6 \times 10^{-24}$, $\frac{\Delta}{k_B T_c} = 1.9$, $R_0 = 2.2$ nΩ, and (2) EP + baking: $A = 2.1 \times 10^{-24}$, $\frac{\Delta}{k_B T_c} = 2.0$, $R_0 = 4.8$ nΩ.

penetrating within the niobium, along microcracks or grain boundaries [26,27]. Less intrinsic contributions also come from defects causing localized heating [26]. Baking is known to increase the first-order term by as much as a factor of 2 in 1.47 GHz elliptical cavities [26,28]. We also see a large increase in this term after baking the FRIB 644 MHz cavity.

Not all contributions to the second-order term are known, and it is not the aim of this paper to investigate these. However, we note that possible contributors to the second-order term are the thermal feedback effect and the nonlinear pair breaking effect [26,28]. We did not observe that baking caused significant change in this term, which would further indicate that there was no significant increase in sources of Joule heating or dielectric losses after the baking treatment. With regard to the thermal-feedback effect, we note that the outer surface of the cavity was held in the same thermal environment in each test to mitigate any possible differences in the thermal feedback effect between tests. Recall the EP-only test was conducted after the EP + baking test, after a 40 μm EP reset of the cavity (S65-001).

In the EP-only case, second-order fitting becomes invalid after B_{pk} increases beyond 100 mT, once the high-field Q-slope becomes evident. *In situ* 120 °C baking is known to reduce high-field Q-slope in ILC TESLA cavities, however in the case of the FRIB 644 MHz cavities operating at a gradient of 17.5 MV/m, baking to eliminate the high-field Q slope would not lead to a decrease in R_s until the cavity exceeds a B_{pk} of 110 mT, ~40% higher than its design gradient.

It is noteworthy that the effect of 120 °C baking in the FRIB 644 MHz cavity differs from the effect in 1.3 GHz ILC TESLA cavities, where it is part of typical high-gradient treatment [19,29,30]. At 644 MHz, and a different B_{pk} (an effect of the medium-β geometry), the FRIB upgrade cavity sees a higher contribution of R_0 to R_s than in an ILC TESLA cavity. This is in part due to the fact that the fraction of R_0 due to the trapped magnetic flux scales approximately with the square root of the operating frequency, whereas the R_{BCS} scales with the square of the operating frequency [31]. It is further noteworthy that the operating gradient of the FRIB cavity is lower than the typical high-gradient cavity, such that it falls within the medium-field Q-slope region. As noted, previous studies, both theoretical and experimental, [26,28,32] find that baking increases the medium-field Q slope, and our results confirm this. Due to this consistency, we are unmotivated to pursue baking treatments further in this frequency and gradient regime.

The Argonne EP facilities used to treat the EP-only and the EP + Baking cavity are well-established and have shown good consistency in cavity performance curves [33,34] over the last decade, giving the authors confidence in the statistical relevance of the results obtained from the FRIB EP cavity test.
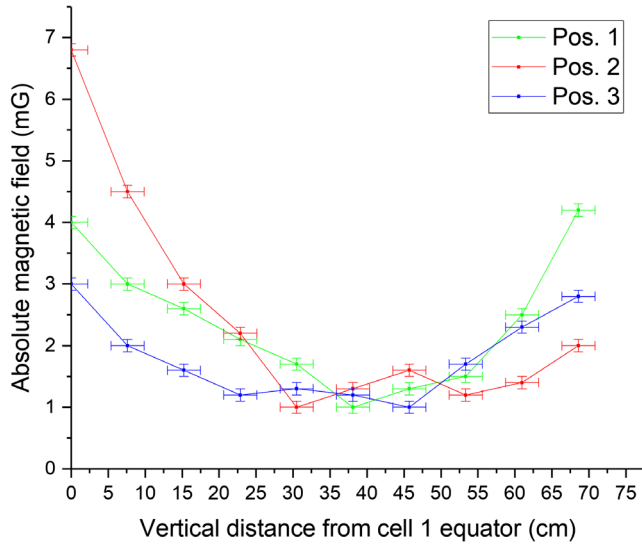
FIG. 4.   Background magnetic field in the vertical test dewar. The fields were measured by lowering fluxgate magnetostatic sensors in increments to create a vertical scan at three different horizontal positions. The sensor locations were offset from the center axis by the same distance as the cavity equator, and they are spaced by 120° in the azimuthal direction from each other. These were measured with the cavity installed in the dewar together with the dewar lid; however, this measurement could only be conducted at room temperature, not at 2K.
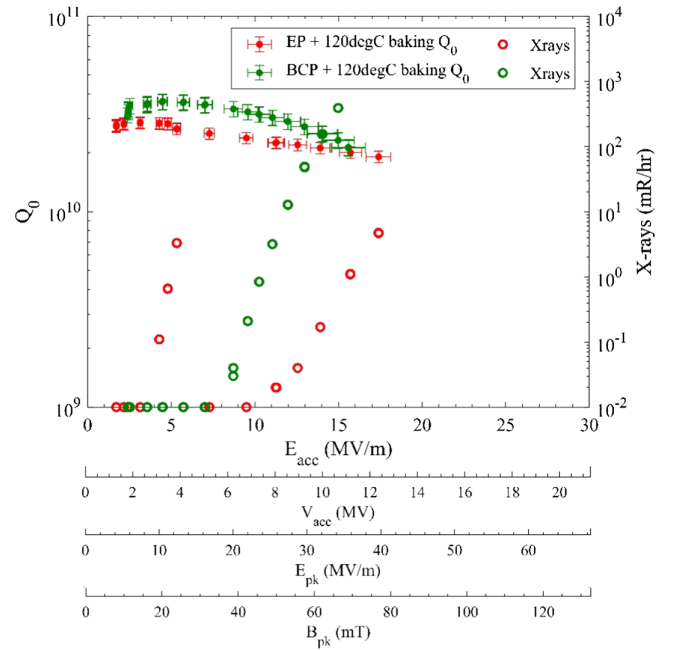

FIG. 5.   Results of the high-power rf testing of 644 MHz $\beta_{\rm opt} = 0.65$ cavities at MSU/FRIB. 2 K Q curves of the BCP + 120 °C baking treatment (green) compared to the previous EP + 120 °C baking treatment (red). The maximum gradient was limited in the BCP + baking test by field emission. The open circles depict field-emission x rays, read on the right-hand vertical scale.

The background magnetic field was below 7 mG for all locations in these tests, with an average of 2.23 mG as shown in Fig. 4. Despite the low average background field, the first and fifth cells are subject to elevated, and potentially problematic, background fields given the sensitivity of these cavities to flux trapping. This will be especially true after planned N-doping, and will be addressed using compensation coils in future tests to more uniformly minimize the background magnetic field.

The 2 K Q-curve of the BCP + baking treatment is shown in Fig. 5 juxtaposed with the EP + baking results. The BCP + baking cavity shows a relatively strong low-field Q-slope, which appears as an inverse Q-slope at $B_{\rm pk}$ lower than approximately 20 mT. As a result, the BCP + baking cavity's Q_0 values below 60 mT exceed the EP + baking Q_0 values at the same field levels. However, a stronger medium-field Q-slope is seen in the BCP + baking cavity, and its Q_0 values are clearly beginning to dip below those of the EP + baking cavity before reaching the FRIB upgrade operating gradient of 17.5 MV/m. Field emission in the BCP + baking cavity prevented testing above 15.6 MV/m at 2 K; however, this field emission was not the cause of the Q-drop observed in that cavity since x-ray degradation of Q_0 begins at an emission level above approximately 100 mR/h, which is well above our measured x-ray emission level. We thus conclude that the measured Q_0 in this cavity up to $E_{\rm acc} = 14$ MV/m or

$B_{\rm pk} = 62$ mT is valid to compare against other rf surface treatments.

Despite the generally inferior performance we observed, 120 °C baking can still impart some benefits that do not manifest in the Q-curves, namely a reduction in multi-pacting (MP) strength. However, in the EP-only case, MP behavior was minimal and strong or hard MP barriers in the MP band were not encountered. The measured MP band for this cavity is centered at $E_{\rm acc} = 10$ MV/m or $B_{\rm pk} = 44$ mT, which corresponds to first-order two-point MP at the cell equators. The first-order two-point MP resonance condition on a 'flat-like' surface is

$$\omega_R = \frac{eB_{\rm pk}}{m_e} = 2\omega_{\rm rf}, \qquad (4)$$

where ω_R is the angular electron cyclotron resonance frequency at a given $B_{\rm pk}$, e, and m_e are the charge and mass of electron, $\omega_{\rm rf}$ is the angular rf frequency [31]. At 644 MHz, this resonance condition occurs at $B_{\rm pk} = 46$ mT, which is roughly consistent with the MP band we measured at $B_{\rm pk} = 44$ mT. Further, this field-strength associated with this equator MP band at 644 MHz is similar to the field-strength associated with the equator MP band in 1.3 GHz TESLA cavities, if scaled to that frequency [34]. Fig. 6 shows an example of the 644 MHz MP band conditioning period. With gradual increases of the forward rf power, MP
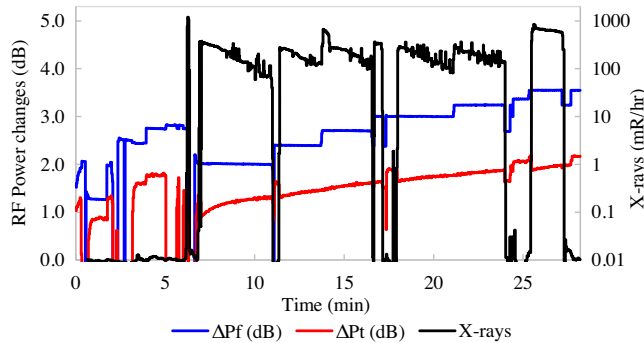
FIG. 6. RF conditioning of the cavity multipacting in the EP-only test. Pf and Pt are the forward and transmitted rf powers, respectively. The MP started to appear at an E_{acc} of 9.3 MV/m ($t = 0.3$ min in this plot). The first three sudden drops of Pt ($t < 5$ min) are due to the MP-induced thermal breakdown with no X-rays. After these events, X-rays were detected and we performed rf conditioning increasing the Pf stepwise. The MP was thoroughly conditioned and disappeared at an E_{acc} of 10.4 MV/m ($t = 28$ min). The X-ray detector was located to the side of the vertical test dewar, within 1 m from the cavity.

was successfully conditioned within 30 min. MP strength in principle depends not only on cavity geometry but also on the cleanliness of the cavity's inner surface and the cavity vacuum quality. Since this moderate MP band was overcome with standard FRIB surface cleaning procedures and vacuum systems, we do not expect MP will be a significant issue in this style of cavity.

III. MECHANICAL MODE STUDIES

Anticipating cryomodule integration, the FRIB upgrade cavity's mechanical modes are important to consider, particularly in FRIB's continuous-wave cryomodules, which generally have relatively high loaded Q (Q_L) compared to pulsed cryomodules. Mechanical modes sensitive to the cavity's operating frequency of 644 MHz

can potentially drive resonant microphonics and ponder-omotive instabilities [35,36,37,38]. The design of the FRIB upgrade cavity includes stiffening rings to reduce mechanical vibrations within the cavity and reduce its displacement sensitivity to the rf resonant frequency. The steep sidewalls of the FRIB upgrade cavity make it particularly susceptible to an "accordion" or longitudinal mode compared to the TESLA cavity shape, whose side-walls are much less steep with a more rigid cell.

The mechanical simulations predicted the mechanical resonances including the transverse cavity modes at 72 and 91 Hz, the cavity-bellows accordion mode at 94 Hz, the cavity twist mode at 123 Hz [2]. The cavity-bellows accordion mode is expected to be the dominant mechanical mode, strongly coupled to the rf frequency. Usually, cavity mechanical modes are characterized in cold tests with helium-jacketed cavities equipped with tuners and with means to measure the Lorentz transfer function or piezo transfer function. However, as we were interested in the cavity mechanical mode of this new shape cavity, particu-larly damping of the accordion mode, the mechanical modes were measured using the available undressed five-cell cavities on a test bench at room temperature [39]. The undressed cavity was fitted with two adjustable but rigid stainless steel bars clamped to the ends of the cavity, as shown in Fig. 7, effectively pinning the ends as if a helium jacket were present. In the accordion mode, this frame provides the same constraints as the real helium jacket since the displacements are in the longitudinal direction. In the other mechanical modes such as the transverse and twist modes, their amplitudes may be exaggerated as the frame does not provide the same stiffness against bending or torsion as the real helium jacket; however, these modes are not interesting modes in this measurement since they are not strongly coupled to the rf frequency. A mechanical speaker was then fitted to the cavity test stand, and driven with a sine wave scanning from 0 to 200 Hz. 200 Hz was chosen as a maximum because
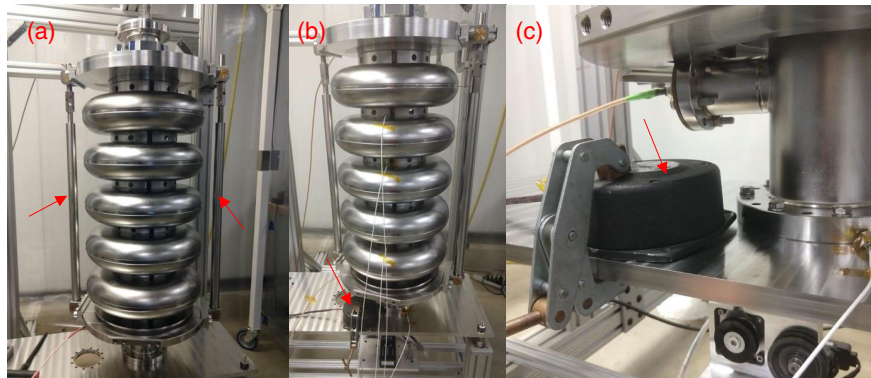

FIG. 7. (a) 644 MHz cavity assembled with the rigid steel bars (arrows) clamped to the ends of the cavity to mimic the presence of the helium jacket. (b) Cavity assembled on the test stand with the mechanical speaker (arrow) in place, with accelerometers (white cables) attached to the cell equators. (c) details of the mechanical speaker coupled to the cavity test stand.

possible external microphonics disturbances other than the cavity mechanical modes are within the range up to several tens of Hz based on experience with the FRIB cryomodules. Furthermore, simulations predict the FRIB upgrade cavity "accordion mode" is at 95 Hz [2,40].

While the cavity was being mechanically scanned, the cavity accelerating rf mode was excited and the sidebands were measured on a real-time spectrum analyzer, which provides 0.1 Hz minimum resolution bandwidth. As the scan progressed, the dominant resonance coupled to the rf mode appeared at 96 Hz as shown in Fig. 8, consistent with predictions. Accelerometers attached to the cavity cells show sinusoidal oscillations with a phase advance per cell as shown in Fig. 9, roughly consistent with the predicted accordion mode [2,41]. We also measured the decay time of

FIG. 9. Displacement oscillations at the 95 Hz mechanical mode. These are measured from the accelerometers attached on the equators and aligned to the cavity axis (longitudinal direction). The phase advances are 28° from Cell #1 to Cell #2, −4° from Cell #2 to Cell #3, 52° from Cell #3 to Cell #5.
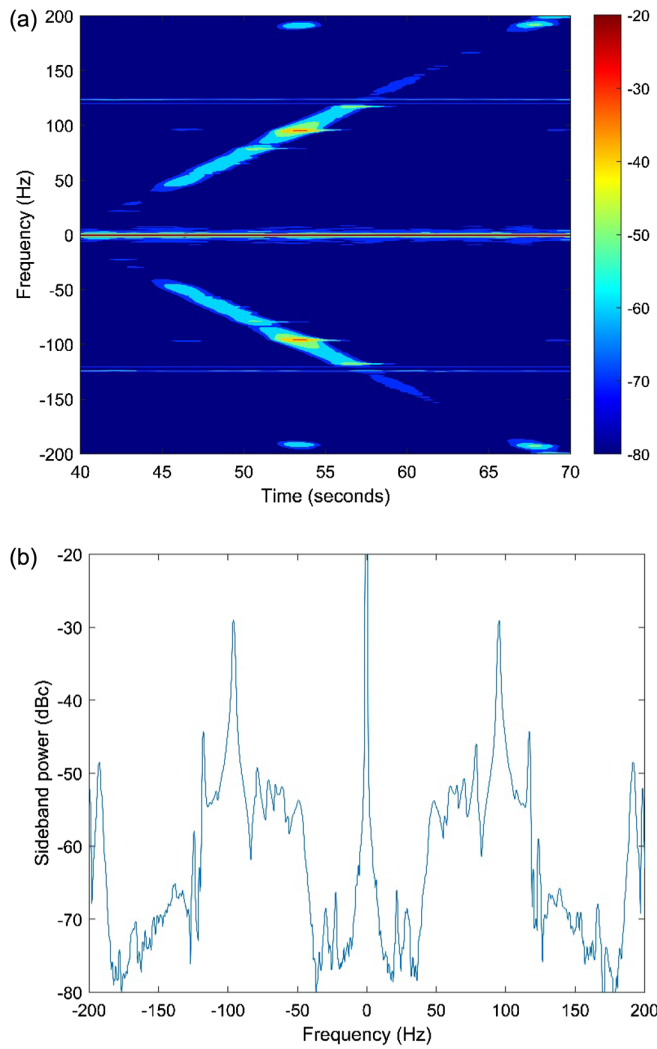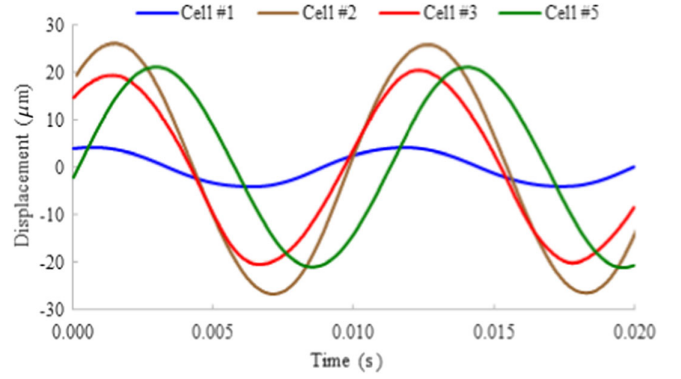

FIG. 8. (a) The spectrogram with the mechanical mode scan. Sinusoidal vibrations were excited and its frequency was swept from 20 to 200 Hz. The color map represents the sideband power in units of dBc. (b) The integrated spectrum. The dominant electromechanical resonance is at 96 Hz, with a response at least 15 dB stronger than any other mode.

this sideband to characterize the mechanical mode Q factor. The measured decay time is −14 dB/sec as shown in Fig. 10 which yields the mechanical Q of 185. This mechanical mode Q is no higher than that in 1.3 GHz TESLA cavities or FRIB $\beta_{\mathrm{opt}} = 0.53$ 322 MHz half-wave resonators [40,41].

The relationship between the rf sideband decay time and the mechanical mode Q was derived as follows: when the accordion mode is excited with the displacement amplitude Δx, the rf resonant frequency oscillates with the frequency excursion amplitude Δf, which results in the phase modulation with amplitude $\Delta\phi$ in the rf circuit. The mechanical displacement is much smaller than the cavity size, thus $\Delta f \propto \Delta x$. The frequency excursion is much smaller than the room temperature cavity rf bandwidth, thus $\Delta\phi \propto \Delta f$ and $\Delta\phi \ll 1$. The first sideband "power" is proportional to $J_1^2(\Delta\phi)$, where $J_1(x)$ is the first-order Bessel function with argument x. Since $\Delta\phi \ll 1$, the sideband power is approximately proportional to $\Delta\phi^2$ and thus proportional to Δx^2. Therefore, the decay time of the rf sideband power is the same as the decay time of the energy of the mechanical oscillation and the mechanical mode Q factor Q_m can be represented by

$$Q_m = \omega_m \tau_{\mathrm{SB}}, \qquad (5)$$

where ω_m is the modulation frequency and τ_{SB} is the exponential decay time of the first rf sideband power.

IV. DISCUSSION

We find herein that the FRIB 644 MHz $\beta_{\mathrm{opt}} = 0.65$ five-cell elliptical cavity meets and exceeds FRIB upgrade goals for Q_0 and E_{acc} with an EP-only treatment, and thus is a suitable candidate cavity design in which to develop future high-Q treatments such as N-doping for the FRIB400 upgrade. With a cavity Q_0 of 2.3×10^{10} at 17.5 MV/m
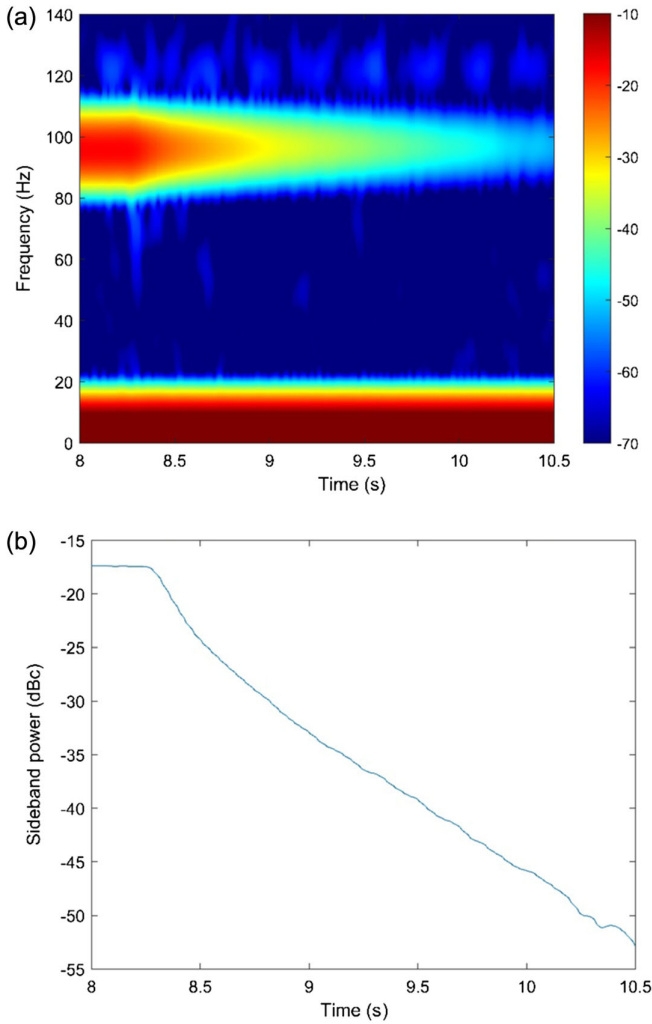
FIG. 10. (a) Spectrogram of the decay time measurement of the dominant 95 Hz mechanical sideband mode. This mode was excited with the mechanical speaker, which was shut off at $t = 8.25$ s. The color map represents the sideband power in the unit of dBc. (b) The decay curve measured at 95 Hz. The decay rate of the mechanical mode energy is -14 dB/s.

and an R/Q of 368 Ω, we calculate the dynamic heat load for a single cavity to be 18.2 W, falling within the design budget of 20 W [2].

We found that 120 °C baking did not improve the cavity performance at 17.5 MV/m of either the BCP or EP treatments. Since 17.5 MV/m resides well within the region of the Q-curve dominated by the medium-field Q-slope, 120 °C baking would have had to reduce the MFQS to improve cavity performance at this operating gradient. However, as in both theoretical and experimental studies [26,28,32] it has been established that 120 °C baking increases the MFQS, and our results confirm these findings, which, in theory, would not motivate further pursuit of this treatment for high-Q_0 at 17.5 MV/m if this had been of interest.

While 120 °C baking is known to reduce R_{BCS}, we show that it increases the cavity R_0, which is the dominant contributor to R_S at the FRIB cavity operating temperature of 2 K. With the FRIB cavity operating at 644 MHz and B_{pk} of 77.5 mT, it is significant that the portion of the residual resistance due to the trapped magnetic flux (R_H) scales with the square root of the operating frequency, whereas R_{BCS} scales with the square of the operating frequency. Thus, higher-frequency cavities suffer more from R_{BCS} and suffer less from R_H contributions to R_0. Higher frequency cavities thus benefit more by 120 °C baking than the 644 MHz cavity tested in this work.

120 °C baking is also known to mitigate the high-field Q-slope. However, in a conservative estimation, the FRIB 644 MHz cavity would not see improvements in Q from mitigation of the high-field Q-slope until the cavity operating gradient increases beyond at least 26 MV/m, which is not an operational possibility.

Regarding the stability of the resonance control, the low-frequency accordion mode of the undressed cavity was measured and found to be weakly powered and of a smaller Q than other mechanical modes observed in the other cavities currently installed and operating in the FRIB linac. This is a promising result as the dominant mechanical mode will not be resonantly built up by external vibrations (microphonics) or interaction with the Lorentz force detuning effect (ponderomotive instability). The next step in the resonance control study is characterizing the dynamic Lorentz force detuning effect in helium jacketed cavities. The final goal is validating the stability of the resonance control in a cryomodule fully integrated with the low-level rf control and cryogenics systems.

Readers may note that several cold tests revealed early onset of field emission: only one test achieved high gradient (26 MV/m) without it. Detailed analysis of the rf surface processing and clean assembly procedures at MSU revealed that the existing robotic HPR system, developed for the FRIB half-wave resonators (HWRs), was sub-optimal for the large elliptical cavity shape, and was the most likely cause of the field emission. The main drawback of the HPR system was the limited sweep angle of the rinsing wand which resulted in using a relatively large number of nozzles (18) with lower jet speeds. The reduction from 18 to 12-hole nozzles and improved programming of the wand motion through the cavity pushed the onset of field emission from mid-E_{acc} range upward to 25 MV/m. Currently, this HPR system is being modified for better accommodation of the multicell low-frequency elliptical cavities. A rotational HPR system enables continuous rotation of the cavity, which in turn allows the number of water jet nozzles to be reduced to only 2 or 3, increasing the jet velocity and improving other parameters such that uniform coverage of all rf surfaces can be achieved. In HPR processing at ANL in collaboration with FNAL and ANL, in preliminary investigation of nitrogen doping, no field

emission was observed in these cavities after surface processing in these facilities. This demonstrates that despite the larger cavity diameters and the steeply sloping side-walls, it is possible to process them to a field emission-free state.

Since the conclusion of this study, further EP data have been collected in field-emission free trials, and no significant change is observed in the rf performance, proving the FE reported herein was not the cause of lower Q in EP-only cavity trial.

Even though the EP with the current cathode achieved remarkable cavity performance, the uniformity of surface removal with the EP is not fully optimized yet. As it is claimed that the performance of the nitrogen-doped cavities is sensitive to the thickness of the post EP, further study on the uniformity of surface removal and improvements in the cathode design could be important for future high-Q R&D with advanced surface treatments such as nitrogen doping.

At this point, additional effort will be needed to repeat the performance of the undressed cavity in a jacketed cavity, and then in turn, in an FRIB Energy Upgrade cryomodule. In the course of this, more development and integrated testing of the cavity and cryomodule subsystems will be needed. These include fast/slow piezo and mechanical tuner studies, with the goal of improving the dynamic range and operational lifetimes of these devices before application in an FRIB energy upgrade cryomodule [2,42,43]. Ultimately, full integration and testing with the cryogenics system and cryomodule assembly will be required to establish how well the integrated cavity performance compares to the undressed cavity performance described here.

Despite meeting the minimum upgrade requirements in terms of Q_0 and E_{acc}, there is strong motivation to proceed with advanced surface treatment studies for these cavities, in particular, with N-doping. N-doping in other frequency and velocity regimes has proven a strong candidate for increasing cavity Q_0, especially in 1.3 GHz TESLA cavities [5,6,7], however, more work is needed to understand how to adapt successful N-doping techniques to different frequency and velocity regimes. Initial studies of N-doping as a function of cavity frequency have found that N-doping in the 650 MHz range using a "2/6" recipe (2 min nitrogen infusion, 6 min annealing at high temperature) increased the cavity's BCS resistance as a function of field, whereas for 1.3, 2.6, and 3.9 GHz, BCS resistance decreased as a function of field, with the size of the drop increasing with the operating frequency [43]. This amounts to a removal of the classic "anti-Q slope" associated with N-doping, which is detrimental as this anti-Q slope is necessary to achieve the multiple-factors of Q improvement we seek in this cavity and with this treatment. However, the mechanism of N-doping is not well understood as a function of frequency, and development is needed to understand how to optimize N-doping recipes and post N-doping EP treatment for the FRIB Energy Upgrade cavity in this frequency and velocity range. We therefore regard the prototype cavities as an additional opportunity to study the fundamental physics of the frequency dependence of the N-doping technique [43,44]. An understanding of this dependence and how to manipulate it will be broadly useful in designing N-doping recipes for a range of cavities for a range of applications where high-Q will be useful in experimental physics as well as in industry.

V. CONCLUSIONS

At the conclusion of this study, we find that the novel FRIB400 prototype 644 MHz five-cell elliptical medium-β cavity achieves acceptable performance with conventional rf surface processing techniques, proving that the cavity and its novel geometry are sound candidates for future high-Q rf surface processing development. The cavity is currently capable of meeting the design goal of the FRIB energy upgrade with EP-only surface treatment. At the FRIB operating gradient of 17.5 MV/m, the EP-only trial gave a higher Q_0 than the EP + baking recipe due to lower residual resistance and a lower medium-field Q slope. Concerns about MP and mechanical modes introduced by a new cavity shape were alleviated based on the results we present here. MP conditioning was completed in the continuous-wave mode and did not require additional pulsed conditioning. The cavity's accordion mechanical mode Q is somewhat similar to that of the TESLA cavity and it is lower than that in the existing FRIB low-β cavities, which is a promising result regarding the stability of the resonance control since the dominant mechanical mode will not be resonantly built up by microphonics or ponderomotive instability.

ACKNOWLEDGMENTS

---

[1] FRIB400 White Paper, https://indico.frib.msu.edu/event/2/attachments/57/292/FRIB400_Final.pdf.

[2] P. N. Ostroumov, C. Contreras, A. S. Plastun, J. Rathke, T. Schultheiss, A. Taylor *et al.*, Elliptical superconducting RF Cavities for FRIB energy upgrade, Nucl. Instrum. Methods Phys. Res., Sect. A **888**, 53 (2018).

[3] B. Aune *et al.*, Superconducting TESLA cavities, Phys. Rev. ST Accel. Beams **3**, 092001 (2000).

[4] K. Saito *et al.*, Superiority of electropolishing over chemical polishing on high gradients, in *Contribution to 8th*

Workshop on RF Superconductivity [*Part. Accel.* 60, 193 (1998)], https://inspirehep.net/literature/470403.

[5] S. Michizono, The International Linear Collider, Nat. Rev. Phys. **1**, 244 (2019), https://doi.org/10.1038/s42254-019-0044-4.

[6] W. Singer *et al.*, Production of superconducting 1.3 GHz cavities for the European x-ray free electron laser, Phys. Rev. Accel. Beams **19**, 092001 (2016).

[7] A. Grassellino, A. Romanenko, D. Sergatskov, O. Melnychuk, Y. Trenikhina, A. Crawford, A. Rowe, M. Wong, T. Khabiboulline, and F. Barkov, Nitrogen and argon doping of niobium for superconducting radio frequency cavities: A pathway to highly efficient accelerating structures, Supercond. Sci. Technol. **26**, 102001 (2013).

[8] A. Grassellino *et al.*, Unprecedented quality factors at accelerating gradients up to 45 MV/m in niobium superconducting resonators via low temperature nitrogen infusion, Supercond. Sci. Technol. **30**, 094004 (2017).

[9] D. Gonnella, R. Eichhorn, F. Futura, M. Ge, D. Hall, V. Ho *et al.*, Nitrogen-doped 9-cell cavity performance in a test cryomodule for LCLS-II, J. Appl. Phys. **117**, 023908 (2015).

[10] D. Gonnella, S. Aderhold, A. Burrill, E. Daly, K. Davis, A. Grassellino *et al.*, Industrialization of the nitrogen-doping preparation for SRF cavities for LCLS-II, Nucl. Instrum. Methods Phys. Res., Sect. A **883**, 143 (2018).

[11] Z. A. Conway, A. Barcikowski, G. L. Cherry, R. L. Fischer, S. M. Gerbick, C. S. Hopper *et al.*, Achieving high peak fields and low residual resistance in half-wave cavities, in *Proceedings of SRF 2015* (JACoW, Geneva, 2015), p. 973, https://accelconf.web.cern.ch/SRF2015/.

[12] T. Xu, K. Saito, H. Ao, B. Bird, N. K. Bultman, F. Casagrande *et al.*, Progress of FRIB SRF production, in *Proceedings of SRF2017* (JACoW, Geneva, 2019), p. 345, https://accelconf.web.cern.ch/napac2019/.

[13] W. Hartung *et al.*, Large-scale dewar testing of FRIB production cavities: Results, in *Proceedings of NAPAC 2019* (Lansing, MI, USA, 2019), MOPLO17.

[14] L. Lilje, High gradients in superconducting multi-cell cavities, *in Proceedings of 11th Workshop on RF Superconductivity (SRF'03)* (JACoW, Geneva, 2003), p. 220, https://accelconf.web.cern.ch/SRF2003/INDEX.htm.

[15] M. Drury, E. Daly, G. K. Davies, J. R. Delayen, C. Grenoble, R. Hicks *et al.*, Overview of SNS Cryomodule Performance, in *Proceedings of 2005 Particle Accelerator Conference (Knoxville, Tennessee, 2005)*.

[16] A. Bosotti, A. Bellandi, M. Bertucci, A. Bignami, J. F. Chen, C. G. Maiano *et al.*, Vertical Tests of ESS Medium β Prototype Cavities at LASA., *Proceedings of IPAC17 (Copenhagen, Denmark, 2017)*, MOPVA063.

[17] M. Kelly and T. Reid, Surface processing for bulk niobium superconducting radio frequency cavities, Supercond. Sci. Technol. **30**, 043001 (2017).

[18] C. Z. Antoine, A. Aspart, M. Berthelot, Y. Gasser, J. P. Poupeau, and V. Valin, Morphological and Chemical Studies of Nb Samples After Various Surface Treatments, in *Proceedings of SRF99 (Santa Fe, New Mexico, 1999)*, p. 295, TUP035.

[19] M. Bertucci, A. Bosotti, A. D'Ambros, P. Michelato, L. Monaco, C. Pagani *et al.*, Electropolishing of PIP-II low β cavity prototypes, in *Proceedings of SRF2019 (Dresden, Germany, 2019)*, MOP057.

[20] G. Ciovati, G. Myneni, F. Stevie, P. Maheshwari, and D. Griffis, High field Q slope and the baking effect: Review of recent experimental results and new data on Nb heat treatments, Phys. Rev. Accel. Beams **13**, 022002 (2010).

[21] J. Mammosser, J. Delayen, J. Gordon, L. Phillips, A. M. Valente, T. Wang, A. T. Wu, and J. Saunders, Status of the production electropolishing system at JLab, in *Proceedings of 2003 Particle Accelerator Conference (2003)*, p. 2860.

[22] M. S. Champion, R. A. Dean, J. D. Galambos, M. P. Howell, M. A. Plum, and B. W. Riemer, Progress on the proton power upgrade of the spallation neutron source, in *Proceedings of IPAC2017* (2017), p. 2445.

[23] L. Merminga, *Building for Discovery: The PIP-II Project* (ORNL Virtual seminar, 2021).

[24] H. Padamsee, *RF Superconductivity: Science, Technology, and Applications*, (WILEY-VCH Verlag GmbH & Co. KGaA, Weinheim, 2009), ISBN: 978-3-527-40572-5.

[25] D. Dotson, M. Drury, R. May, and C. Reece, Use of simple x-ray measurements in the performance analysis of cryogenic RF accelerator cavities, Report No. Jlab-ACC-96-11, 1996, https://www.jlab.org/div_dept/admin/publications/papers/96/ACC96-11.pdf

[26] G. Ciovati and J. Halbritter, Analysis of the medium field Q-slope in superconducting cavities made of bulk niobium, Physica (Amsterdam) **441C**, 57 (2006).

[27] J. Halbritter, Transport in superconducting niobium films for radio frequency applications, J Appl. Phys. **97**, 083904 (2005).

[28] G. Ciovati, High Q at Low, and Medium Field, in *Proceedings of Argonne Frontier Workshop (2005)*, edited by K. Kim *et al.* (JLab MIS portal, 2005), p. 52, https://misportal.jlab.org/ul/publications/downloadFile.cfm?hyperlink=ACF2B2C.pdf.

[29] G. Ciovati, P. Kneisel, and A. Gurevich, Measurement of the high-field Q drop in a high-purity large-grain niobium cavity for different oxidation processes, Phys. Rev. Accel. Beams **10**, 062002 (2007).

[30] P. Dhakal, G. Ciovati, and G. Myneni, Role of thermal resistance on the performance of superconducting radio frequency cavities, Phys. Rev. Accel. Beams **20**, 032003 (2017).

[31] H. Padamsee, *RF Superconductivity for Accelerators* (WILEY-VCH Verlag GmbH & Co. KGaA, Weinheim, 2008), ISBN: 978-3-527-40842-9.

[32] J. Vines, Y. Xie, and H. Padamsee, Systematic trends for the medium field Q slope, in *Proceedings of the 13th International Conference RF Superconductivity (SRF'07) (Beijing, China 2007)*, TUP27.

[33] L. Lilje, D. Reschke, K. Twarowski, P. Schmüser, D. Ploess, E. Haebel *et al.*, Electropolishing and in-situ baking of 1.3 GHz niobium cavities, in *Proceedings of 1999 Workshop on RF Superconductivity (Santa Fe, New Mexico, USA)*.

[34] P. Yla-Oijala, Electron multipacting in TESLA cavities and input couplers, Part. Accel. **63**, 105 (1999), https://inspirehep.net/literature/514939.

[35] J. Delayen, Ponderomotive instabilities and microphonics— a tutorial, Physica (Amsterdam) **441C**, 1 (2006).

[36] S. Kim, RF commissioning of the first three Beta=0.041 quarter wave resonator cryomodule in FRIB driver linac, in *Second Topical Workshop on Microphonics* (New York, NY, 2018).

[37] L. Yang, V. Zvyagintsev, R. E. Laxdal, and B. Waraich, Damping of vibrations in superconducting quarter wave resonators, Phys. Rev. Accel. Beams **22**, 030103 (2019).

[38] Y. Pichalnikov, FNAL tuners: LCLS-II to PIP-II, *Second Topical Workshop on Cryomodule Microphonics and Resonance Control* (New York, NY, 2018).

[39] S. Kim, Resonance control with pneumatic slow frequency tuners for FRIB half-wave resonators, *TESLA Technology Collaboration Meeting 2020* (Geneva, Switzerland, 2020).

[40] L. Lilje, S. Simrock, and D. Kostin, Characteristics of a fast piezo-tuning mechanism for superconducting cavities, in *Proceedings of EPAC 2002* (EPAC, 2002), p. 2256, https://accelconf.web.cern.ch/e02/default.htm.

[41] O. Kononenko, C. Adolphsen, Z. Li, C.-K. Ng, and C. Rivetta, 3D multiphysics modeling of superconducting cavities with a massively parallel simulation suite, Phys. Rev. Accel. Beams **20**, 102001 (2017).

[42] M. Martinello, S. Aderhold, S. K. Chandrasekaran, M. Checchin, A. Grassellino, O. Melnychuk *et al.*, Advancement in understanding of the field and frequency dependent microwave surface resistance of Niobium, in *Proceedings of SRF 2017* (JACoW, Geneva, 2017), arXiv:1707.07582, https://accelconf.web.cern.ch/srf2017/.

[43] M. Checchin, M. Martinello, A. Grassellino, S. Aderhold, S. K. Chandrasekaran, O. S. Melnychuk, S. Posen, A. Romanenko, and D. A. Sergatskov, Frequency dependence of trapped flux sensitivity in SRF cavities, Appl. Phys. Lett. **112**, 072601 (2018).

[44] M. P. Kelly, S. M. Gerbick, D. Bice, and G. Wu, Electro-polishing at ANL/FNAL, in *Proceedings of SRF2009 (Berlin, Germany)* (2009), THPPO066.